A molecular probe carrying anti-tropomyosin 4 for early diagnosis of cerebral ischemia/reperfusion injury

Teng-Fei Yu[1], Kun Wang[2], Lu Yin[1], Wen-Zhe Li[3], Chuan-Ping Li[4], Wei Zhang[1], Jie Tian[2, 5, *], Wen He[1, *]

https://doi.org/10.4103/1673-5374.357907

Date of submission: March 21, 2022

Date of decision: July 13, 2022

Date of acceptance: September 3, 2022

Date of web publication: October 11, 2022

From the Contents

Graphical Abstract

Structural and ultrasound (US)/photoacoustic imaging (PAI) of cerebral ischemia/reperfusion injury model mice early after injury

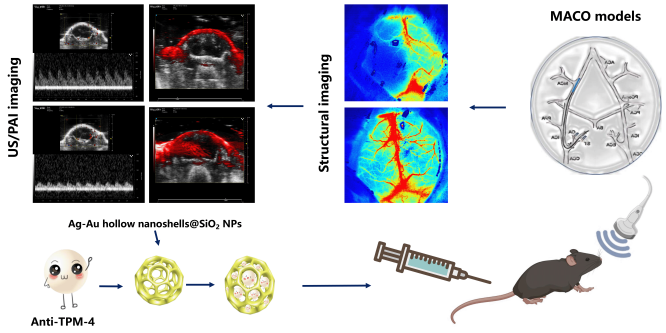

Abstract

In vivo imaging of cerebral ischemia/reperfusion injury remains an important challenge. We injected porous Ag/Au@SiO_2 bimetallic hollow nanoshells carrying anti-tropomyosin 4 as a molecular probe into mice with cerebral ischemia/reperfusion injury and observed microvascular changes in the brain using photoacoustic imaging with ultrasonography. At each measured time point, the total photoacoustic signal was significantly higher on the affected side than on the healthy side. Twelve hours after reperfusion, cerebral perfusion on the affected side increased, cerebrovascular injury worsened, and anti-tropomyosin 4 expression increased. Twenty-four hours after reperfusion and later, perfusion on the affected side declined slowly and stabilized after 1 week; brain injury was also alleviated. Histopathological and immunohistochemical examinations confirmed the brain injury tissue changes. The nanoshell molecular probe carrying anti-tropomyosin 4 has potential for use in early diagnosis of cerebral ischemia/reperfusion injury and evaluating its progression.

Key Words: cerebral ischemia/reperfusion injury; diagnosis; dynamic monitoring; ischemic stroke; middle cerebral artery occlusion; molecular probe; nanoshells; photoacoustic imaging; tropomyosin 4; ultrasound

Introduction

Stroke is classified as either hemorrhagic or ischemic. Ischemic stroke accounts for 85% of all strokes (Saver et al., 2015) and is commonly caused by internal carotid artery stenosis resulting from atherosclerosis. Treatment of acute ischemic stroke is based on reperfusion (Hankey, 2017). However, reperfusion after endarterectomy or stenting may be complicated by cerebral ischemia/reperfusion injury (CISI), which is associated with nearly 50% mortality (Hayakawa et al., 2019). Early diagnosis of CISI and identifying the location of the responsible lesion should enable timely intervention (Emberson et al., 2014; Alper et al., 2015).

Computed tomography and magnetic resonance imaging are used to assess CISI (Provost et al., 2019). However, the time required to acquire and process images can delay treatment (Lutsep et al., 1997; Ryu et al., 2002; Ma et al., 2021). Rapid non-invasive high-resolution imaging techniques with high diagnostic sensitivity are needed. Photoacoustic imaging (PAI) is a relatively new radiation-free imaging technique that might meet this need.

PAI overcomes the problems of resolution and scatter that occur when light is transmitted through solid tissue and offers the contrast of optical imaging and the high resolution of ultrasound (US) imaging at depths of up to several cm (Nie et al., 2014; Liu et al., 2016; Wang and Yao, 2016; Cai et al., 2019). PAI is also useful for studying morphological damage, functional metabolism, and physiological and pathological properties of tissue. Furthermore, it can be used for extended continuous monitoring and has potential for imaging organelles and organs (Zemp et al., 2008; Taruttis et al., 2010; Lv et al., 2018). Moreover, PAI can be performed rapidly, which enables earlier treatment, and can identify hemorrhage, which is important when deciding treatment in the CISI setting.

In a study of localization patterns of myosin heavy chain isoforms in normal arteries and atherosclerotic lesions of increasing severity, Abouhamed et al. reported that during atherogenesis, tropomyosin 4 (TPM4) expression occurs primarily in smooth muscle cells (SMCs) of the synthetic phenotype in the media and intima; furthermore, upregulated TPM4 mRNA is a marker of vascular SMC dedifferentiation (Abouhamed et al., 2003). Nanostructures with discrete metallic, hollow, and porous construction have shown promise in catalysis and nanomedicine applications because of their large surface area, lightweight nature, and broadly tunable localized surface plasmon resonance (Wu et al., 2012). This study aimed to examine the use of anti-TPM4-coated Ag/Au hollow nanoshells@SiO_2 nanoparticles as a PAI contrast agent to diagnose and evaluate CISI in a mouse model of IS (Watson et al., 1985).

Methods

Synthesis of Ag/Au hollow nanoshells

According to a standardized protocol, Ag sol was prepared using the sodium citrate reduction method (Wu et al., 2012). Next, 1.6 mL of 0.1% $HAuCl_4$ and 0.8 mL of 0.02 M NH_2OH were added to 40 mL of Ag nanoparticles (approximately 1.5×10^{11} particles/mL) in a glass vial and mixed using a magnetic stirrer before 5 mL of water was added. Then, a range of volumes (45–550 μL) of 0.1% $HAuCl_4$ and 0.1 mL of 0.02 M NH_2OH were added to the vials and mixed using a magnetic stirrer. After heating and refluxing the solution for a few minutes, it was cooled to room temperature before etching the nanoparticles with 0.1 M H_2O_2 (**Figure 1**).

[1]Department of Ultrasound, Beijing Tiantan Hospital, Capital Medical University, Beijing, China; [2]CAS Key Laboratory of Molecular Imaging, Institute of Automation, Chinese Academy of Sciences, Beijing, China; [3]State Key Laboratory of Natural and Biomimetic Drugs, School of Pharmaceutical Sciences, Peking University, Beijing, China; [4]Anhui Province Key Laboratory of Functional Coordinated Complexes for Materials Chemistry and Application, School of Chemical and Environmental Engineering, Anhui Polytechnic University, Wuhu, Anhui Province, China; [5]Beijing Advanced Innovation Center for Big Data-Based Precision Medicine, School of Engineering Medicine, Beihang University, Beijing, China
*Correspondence to: Wen He, MS, hewen@bjtth.org; Jie Tian, PhD, jie.tian@ia.ac.cn.
https://orcid.org/0000-0002-1452-3529 (Teng-Fei Yu)

Funding: *This study was supported by the National Natural Science Foundation of China, No. 81730050 (to WH).*
How to cite this article: *Yu TF, Wang K, Yin L, Li WZ, Li CP, Zhang W, Tian J, He W (2023) A molecular probe carrying anti-tropomyosin 4 for early diagnosis of cerebral ischemia/reperfusion injury. Neural Regen Res 18(6):1321-1324.*

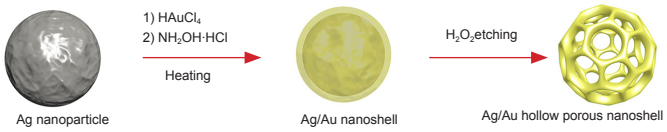

Figure 1 | **Schematic diagram of the Ag/Au hollow nanoshells.**

Synthesis of Ag/Au hollow nanoshells@SiO_2 nanoparticles

Ag/Au hollow nanoshells@SiO_2 nanoparticles were synthesized as described by Li et al. (2017). While vigorously stirring, a suitable amount of 1 mM (3-aminopropyl) trimethoxysilane was added drop by drop to 20 mL of the Ag/Au hollow nanoshells. To ensure complete complexation of amine groups with the gold surface, the mixture was stirred for at least 20 minutes. A sodium silicate solution (0.54 weight percentage) and 0.1 M H_2SO_4 were then added to the solution, which was vigorously stirred then heated at 90°C for 1 hour. After cooling to room temperature, the nanoparticles were centrifuged at 4500 × *g* for 20 minutes and dispersed in 10 mL Milli-Q water (Millipore, Boston, MA, USA). The particles were then transferred to a solution containing 40 mL of ethanol and 1.2 mL of ammonia. After adding 1 mL of 1% tetraethyl orthosilicate, the mixture was stirred at room temperature (25°C) for 24 hours. Subsequently, the nanoparticles were centrifuged and redispersed into 10 mL of isopropanol. Finally, the Ag/Au hollow nanoshells@SiO_2 nanoparticles were carboxylated by adding 3-(triethoxysilyl) propylsuccinic anhydride and heated at 85°C for 24 hours.

Molecular probe synthesis: Ag/Au hollow nanoshells@SiO_2 nanoparticle conjugation with anti-TPM4

1 mL aliquots of nanospheres were first dispersed with US for 15 minutes before 1.5 μL (20 mg/mL) of 1-ethyl-3-(3-dimethylaminopropyl) carbodiimide was added. After reacting at room temperature for 15 minutes, 100 μL of antibody was desalted in a G25 centrifuge column and added to the activated nanospheres. After 30 minutes at room temperature, centrifugation was performed at 6000 × *g* for 10 minutes, and the precipitate was suspended in phosphate-buffered saline. The precipitate was then suspended in Tris-buffered saline for 10 minutes.

Measurement of the photoacoustic effects of *in vitro* samples

To assess PAI *in vitro*, Ag/Au hollow nanoshells@SiO_2 nanoparticle composite nanosheets of different concentrations (0.185–3.0 mg/mL) were dispersed in aqueous solution. The PA images were acquired using a Vevo LAZR photoacoustic imaging system (Visual Sonics, FUJIFILM Inc., Toronto, Canada) equipped with an MX-250 probe. Imaging parameters were as follows: region of interest, 20 mm; frequency, 21 MHz; photoacoustic gain, 35 dB; excitation wavelength, 700 nm.

Animals

C57BL/6N male mice aged 7–8 weeks (specific-pathogen-free level; weight 23 ± 2 g) were obtained from Charles River (Beijing, China, SCXK (Jing) 2016-0006). All *in vivo* studies were conducted according to protocols approved by the Institutional Animal Care and Use Committee at Beijing Tiantan Hospital, Capital Medical University (No. 202102002, on March 26, 2021).

MCAO stroke model

Mice were placed in the supine position and the neck skin was sterilized. The skin was then incised using scissors and elbow ophthalmic forceps were used to passively separate the neck muscles and nerves to visualize the left common carotid artery. Next, the arterial sheath was carefully isolated to avoid injuring the vagus nerve and the exterior and interior carotid arteries were divided. Then, the common and external carotid arteries were ligated with silk thread. The internal carotid artery was gripped with a clip and a small gap was created using ophthalmic scissors. A 6–0 silicone-coated monofilament was then embedded into the common carotid artery and advanced toward the arterial clamp. The filament was held in place with a distal silk tie to remain in place during the occlusion (Fan et al., 2017). Evaluations were performed using the Zea Longa scale (Longa et al., 1989). Three experimenters scored and recorded the mice in a single-blind manner. Mice with scores of 3 to 4 were selected for follow-up experiments.

CISI model

One hour after arterial occlusion, the 6–0 silicone-coated monofilament was extracted to restore cerebral blood flow on the affected side and cause reperfusion injury. Flow was monitored using the RFLSI III laser-speckle blood flow imaging system (RWD, Shenzhen, China) over 168 hours. The experimental timeline with experimental details is shown in **Figure 2**.

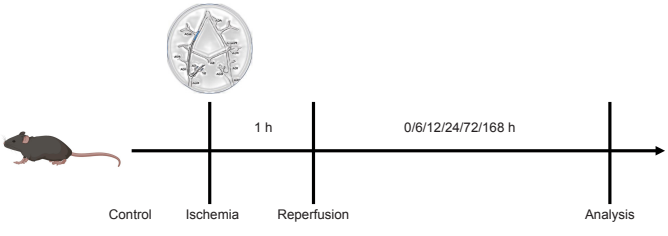

Figure 2 | **Experimental timeline.**

US/PAI detection

A pulse laser integrated with a high-frequency US system (Vevo LAZR-X, VisualSonics, FUJIFILM, Tokyo, Japan) was used to observe microvascular brain changes at the State Key Laboratory of Natural and Biomimetic Drugs, School of Pharmaceutical Sciences, Peking University. Molecular probes were injected into the tail vein immediately and 1, 6, 12, 24, 72, and 168 hours (*n* = 3/time point) after the filament was removed.

Histological analysis

After anesthetizing the mice with 1% isoflurane using a R540IP gas anesthesia machine (RWD), they were sacrificed at specific time points via intracardiac injection of 60 mL of 4% paraformaldehyde. Brains were then removed and stored in 4% paraformaldehyde. Next, the injured areas of the right brain were dissected and embedded in paraffin to prepare a series of adjacent horizontal sections (5 μm thickness). Hematoxylin and eosin staining and immunohistochemical staining were performed to detect the degree of brain tissue damage. Brain tissue was sectioned, air-dried at room temperature, fixed for 30 seconds, stained with hematoxylin (60°C) for 60 seconds, differentiated with 1% hydrochloric acid ethanol, and stained with eosin for 3 minutes. Then, sections were dehydrated using an ethanol series (70%, 80%, 95%, and 100% ethanol; 5 minutes each), cleaned with xylene three times (5 minutes each), and fixed with balsam. The heart was first infused with 0.9% normal saline and then fixed with 4% paraformaldehyde (Sinopac Chemical Reagents, Shanghai, China). After dehydration in 20% sucrose, the left brain injury area was dissected and embedded in paraffin and 5 μm sections were cut using the S700 slicer (RWD). The primary antibody was incubated at 4°C overnight, and the secondary antibody was washed with phosphate-buffered saline and incubated at room temperature for 1 hour (primary antibody, TPM [EPR13316] (1:200, Abcam, Cambridge, UK, Cat# ab181085); secondary antibody, goat anti-rabbit IgG H&L (1:1000, Abcam, Cat# ab6721, RRID: AB_955447)). All sections were scanned using the Pannoramic MIDI scanner (3DHistech, Ltd., Budapest, Hungary). Five fields were randomly selected from each damaged area and ImageJ software version 1.8.0 (National Institutes of Health, Bethesda, MD, USA) was used to quantify integrated optical density (Schneider et al., 2012). The images were reviewed by experienced physicians who were blinded to grouping. The reports were subsequently group-matched by a researcher. Degree of cerebral cortex tissue injury on the affected side was classified as mild, moderate, and severe (Zhao et al., 2014; Ludwig et al., 2018).

Statistical analysis

Sample size was not statistically predetermined; however, our sample sizes were similar to those reported in a previous publication (Rosenkrans et al., 2022). No animals or data points were excluded from analysis. Quantitative data are presented as means ± standard deviation (SD). Statistical analyses were performed using SPSS software version 21 (IBM Corp., Armonk, NY, USA). Groups were compared at different time points using one-way repeated measures analysis of variance. $P < 0.05$ was considered significant.

Results

Characterization of TPM4-targeted Ag/Au hollow nanoshells@SiO_2 nanoparticles

The prepared material showed a nanometer particle with a cage structure and diameter of approximately 80 nm (**Figure 3**). Based on a distribution mapping diagram of the elements O, Au, Si, and Ag, the elements were evenly distributed throughout the nanoparticles. The ultraviolet-visible absorption spectra for Ag/Au and Ag/Au@SiO_2 showed peaks at 808 nm.

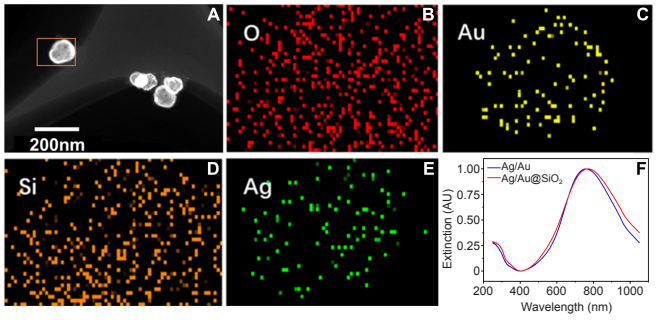

Figure 3 | **Characterization of TPM4-targeted Ag/Au hollow nanoshells@SiO_2 nanoparticles.**

The prepared material showed a nanometer particle with a cage structure and diameter of approximately 80 nm. (A) Transmission electron microscopy image of Ag/Au@SiO_2. Scale bar: 200 nm. (B–E) The corresponding element distribution mapping and energy dispersive spectrometer results. (F) The ultraviolet-visible absorption spectrum for Ag/Au and Ag/Au@SiO_2 showed peaks at 808 nm. AU: Absorbance unit.

Monitoring using laser-speckle blood flow imaging systemand the US/PAI system

During cerebral ischemia, cerebral blood perfusion in the affected (left) side was almost zero on the Zea Longa scale, which indicated successful construction of the ischemia model. After experimental restoration of blood flow, cerebral blood perfusion on the affected side increased over time (**Figure 4A–H**). Change in perfusion significantly differed between the affected

and healthy sides (F = 6.127, degrees of freedom 15, P < 0.05). Change in perfusion was significantly higher at 12 hours compared to other periods then decreased gradually (**Figure 4I**).

Transcranial US examination coupled with the color Doppler flow mode revealed that the blood flow signal of the left middle cerebral artery was apparently weaker than that of the right side. Moreover, the blood flow velocity of the middle cerebral artery was determined by pulsed-wave Doppler and that of the left side was lower than the right one (**Figure 4J–L**).

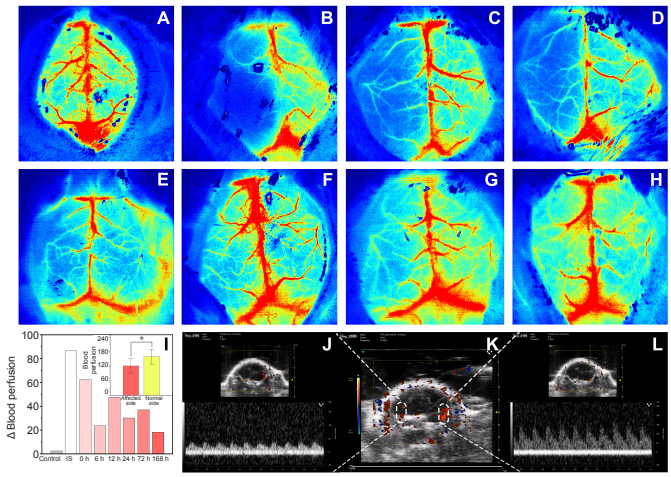

Figure 4 | Monitoring using laser-speckle blood flow imaging system and the ultrasound/photoacoustic imaging system.
(A–H) During cerebral ischemia, cerebral blood perfusion on the affected (left) side was almost zero, which indicated that the ischemia model was successfully constructed. One hour after induction of ischemia, cerebral blood flow was experimentally restored and monitored using a laser-speckle blood flow imaging system over 168 hours. Cerebral blood perfusion in the affected side increased over time: control (A), ischemic stroke (B), before reperfusion (C), 6 hours after reperfusion (D), 12 hours after reperfusion (E), 24 hours after reperfusion (F), 72 hours after reperfusion (G), and 168 hours after reperfusion (H). Red indicates local perfusion. (I) Change in total perfusion differed significantly between the affected and healthy sides in all mice (*P < 0.05); Change in perfusion in control mice, ischemic stroke (IS) mice, and after reperfusion at various time points is also shown. Data are expressed as means ± SD (n = 3) and were analyzed using one-way repeated measures analysis of variance. (J) Pulse wave Doppler showed decreased flow in the left middle cerebral artery. (K) Color Doppler flow imaging showed normal perfusion in the right middle cerebral artery. The perfusion signal in the left middle cerebral artery was thin and discontinuous. (L) Flow in the right middle cerebral artery was normal.

Evaluation of the probe in the mouse CISI model using the US/PAI system

Molecular probes were injected into the tail vein immediately and 1, 6, 12, 24, 72, and 168 hours after removal of the monofilament. Photoacoustic examination was performed immediately after removal and brain reperfusion injury was quantitatively and qualitatively analyzed. As shown in **Figure 5**, the photoacoustic signal was significantly stronger on the affected (left) side than on the healthy (right) side. At 12 hours, the difference in photoacoustic signal between the two hemispheres increased transiently then became gradually smaller over time. At each time point, the total photoacoustic signal was significantly higher on the affected side than on the healthy side (F = 5.045, degrees of freedom = 13, P < 0.05). However, the photoacoustic signal on the affected side did not depend on the time after reperfusion.

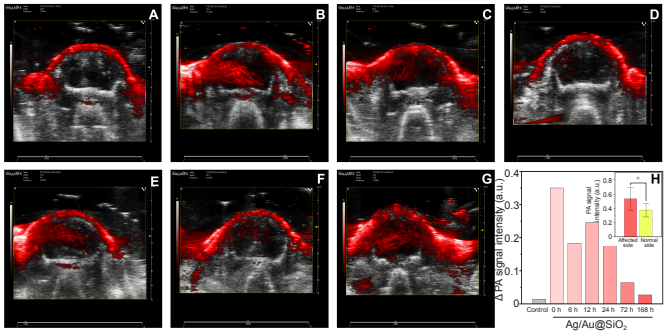

Figure 5 | Photoacoustic imaging with the co-registered ultrasound system was used to evaluate the probe in the mouse model of cerebral ischemia/reperfusion injury.
(A–G) The photoacoustic signal was significantly stronger on the affected side (left) than on the healthy side (right). At 12 hours, the difference in photoacoustic signals between the two hemispheres increased transiently. Control (A), 0- (B), 6- (C), 12- (D), 24- (E), 72- (F), and 168-hour (G) groups. Two-dimensional ultrasound images were used as anatomical background, and the red signal is the photoacoustic signal expressed by molecular probe. (H) Photoacoustic signal of the molecular probe before and 6, 12, 24, 73, and 168 hours after left brain reperfusion. The total molecular probe photoacoustic signal was significantly higher on the affected side (left) than on the healthy side (*P < 0.05). Data are expressed as means ± SD (n = 3) and were analyzed using one-way repeated measures analysis of variance.

Histological analysis in the mouse CISI model

After photoacoustic examination at each time point, the mice were sacrificed and their brain tissue extracted for histological examination. Brain tissue damage was assessed on hematoxylin and eosin-stained slides (**Figure 6**). TPM4 immunohistochemical staining showed tissue damage on the affected side was severe in the 1-, 24-, and 168-hour groups, mild in the 12- and 72-hour groups, and moderate in the 6-hour group (**Figure 7**).

Discussion

Previous ischemic stroke research has concentrated on decreasing hypoperfusion time to maintain brain function (Lee et al., 2018). Nevertheless, clinical results after restoration of blood flow to ischemic brain remain suboptimal. Basic and clinical research have not yet revealed the detailed mechanisms underlying CISI (Silvestri et al., 2017). Understanding these mechanisms may provide a solid basis for developing CISI treatments and preventing brain injury (Wu et al., 2018).

Vascular SMC phenotype governs the properties and functions of the vessel wall. In the tunica media, SMCs are responsible for maintaining vessel wall tone. Enhanced TPM4 mRNA expression is a fiducial differentiation marker for synthetic SMCs (Abouhamed et al., 2003). Because damage to cerebrovascular SMCs can promote TPM4 expression, we prepared and injected a molecular probe carrying anti-TPM4 nanocages into the tail veins of male mice. As in other relevant studies, female mice were excluded to reduce experimental errors caused by the mice themselves (Alamri et al., 2021). In our study, a molecular probe was designed to enter the cerebral vasculature, pass through the vascular endothelial cells and target vascular SMCs. US/PAI was then used to predict and diagnose CISI. Furthermore, the nanocages we prepared are capable of carrying drugs, and therefore may have a role in CISI treatment in the future.

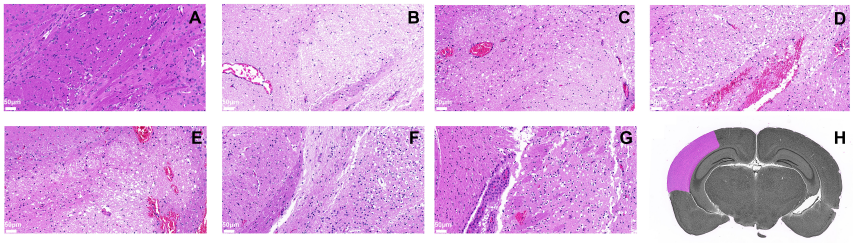

Figure 6 | Pathological analysis of cerebral cortex supplied by the left middle cerebral artery (affected side).
Changes in brain tissue on the affected side were visualized after reperfusion using hematoxylin and eosin staining in the control (A), 0- (B), 6- (C), 12- (D), 24- (E), 72- (F), and 168-hour (G) groups. Scale bars: 50 μm. The vessel walls and brain tissue were severely damaged at 12 to 24 hours after reperfusion and the number of cells in the cortex was decreased. Some cortical neurons were necrotic and degenerated with pyknotic and hyperchromatic nuclei. Some nerve fibers were loosely arranged and irregular with sieve-like structures and many vacuoles. However, 72 hours after reperfusion, the cells had recovered. (H) Schematic diagram of the left middle cerebral artery-supplied cortex.

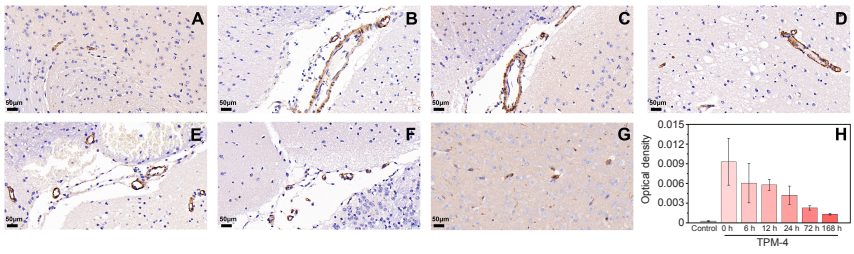

Figure 7 | Tropomyosin 4 (TPM4) immunohistochemical analysis of cortex supplied by the left middle cerebral artery (affected side).
(A–G) Changes in brain tissue on the affected side were visualized after reperfusion using immunohistochemical TPM4 staining in the control (A), 0- (B), 6- (C), 12- (D), 24- (E), 72- (F), and 168-hour (G) groups. Scale bars: 50 μm. (H) Changes in optical density of TPM4 at different periods using immunohistochemical staining. Data are expressed as means ± SD (n = 3) and were analyzed using one-way repeated measures analysis of variance.

US/PAI is a non-ionizing, non-invasive, and real-time imaging technique that has been used in preclinical studies of various diseases (Hu et al., 2021). It has sufficient penetration depth and spatial resolution to detect fine inner organ structures and allow detailed CISI research. Moreover, the molecular probe used in our study is non-toxic. Further developments and improvements upon it should enable human studies in the near future.

Rather than using the conventional molecular probe observation time, we used an observation method that was in line with the contrast-enhanced US procedure: brains were observed immediately after intravenous injection. Because nanomaterials are absorbed by brain tissue itself, we examined blood perfusion volumes and TPM4 expression in both affected (ischemic) and healthy tissue. Early after reperfusion of ischemic brain, the vessel walls and brain tissue were severely damaged and the number of cortical cells was decreased. Some nerve cells in the cortex were necrotic and degenerated with pyknotic and hyperchromatic nuclei. In addition, some nerve fibers were loosely arranged and irregular with sieve-like structures and many vacuoles. Leakage of blood cells was also observed. At the same time, TPM4 expression in the cerebrovascular wall was significantly increased. It was not until 24 hours after reperfusion that self-regulation and self-repair was observed, and the degree of damage gradually decreased. The injured state gradually recovered within a week, although the brain tissue structure remained slightly abnormal: punctate liquefaction necrosis in the cortex and a small degree of cell edema were observed. Nucleoli in a few cells disappeared and more vacuoles were present. The expression of TPM4 in the cerebrovascular wall also decreased gradually.

We successfully constructed a molecular probe of porous Ag/Au@SiO_2 bimetallic hollow nanoshells carrying anti-TPM4 for the early diagnosis and dynamic monitoring of CISI using US/PAI. These nanoshells successfully served as a contrast agent for PAI and have potential to carry and release drugs *in vivo* because of their unique cage structure. This probe shows promise for use in early diagnosis of CISI and assessment of its complications and progression. And then, early intervention of reperfusion injury can reduce the complications and mortality after recanalization. Further studies are warranted, as our study is only preliminary.

Author contributions: *Study conceptualization, resources, project administration and funding acquisition: WH, JT; methodology: TFY, KW; software: LY; validation, formal analysis: TFY, WH, KW; investigation: TFY, WH, JT; formal analysis, manuscript draft: TFY; data curation, visualization: TFY, LY; manuscript review and editing: TFY, WZL, CPL, WZ, KW, WH; supervision: KW, WH. All authors have read and agreed to the published version of the manuscript.*
Conflicts of interest: *There are no conflicts to declare.*

References

Abouhamed M, Reichenberg S, Robenek H, Plenz G (2003) Tropomyosin 4 expression is enhanced in dedifferentiating smooth muscle cells in vitro and during atherogenesis. Eur J Cell Biol 82:473-482.

Alamri FF, Al Shoyaib A, Syeara N, Paul A, Jayaraman S, Karamyan ST, Arumugam TV, Karamyan VT (2021) Delayed atomoxetine or fluoxetine treatment coupled with limited voluntary running promotes motor recovery in mice after ischemic stroke. Neural Regen Res 16:1244-1251.

Alper BS, Malone-Moses M, McLellan JS, Prasad K, Manheimer E (2015) Thrombolysis in acute ischaemic stroke: time for a rethink? BMJ 350:h1075.

Cai C, Wang X, Si K, Qian J, Luo J, Ma C (2019) Feature coupling photoacoustic computed tomography for joint reconstruction of initial pressure and sound speed in vivo. Biomed Opt Express 10:3447-3462.

Emberson J, Lees KR, Lyden P, Blackwell L, Albers G, Bluhmki E, Brott T, Cohen G, Davis S, Donnan G, Grotta J, Howard G, Kaste M, Koga M, von Kummer R, Lansberg M, Lindley RI, Murray G, Olivot JM, Parsons M, et al. (2014) Effect of treatment delay, age, and stroke severity on the effects of intravenous thrombolysis with alteplase for acute ischaemic stroke: a meta-analysis of individual patient data from randomised trials. Lancet 384:1929-1935.

Fan J, Li Y, Fu X, Li L, Hao X, Li S (2017) Nonhuman primate models of focal cerebral ischemia. Neural Regen Res 12:321-328.

Hankey GJ (2017) Stroke. Lancet 389:641-654.

Hayakawa M, Sugiu K, Yoshimura S, Hishikawa T, Yamagami H, Fukuda-Doi M, Sakai N, Iihara K, Ogasawara K, Oishi H, Ito Y, Matsumaru Y (2019) Effectiveness of staged angioplasty for avoidance of cerebral hyperperfusion syndrome after carotid revascularization. J Neurosurg doi: 10.3171/2018.8.JNS18887.

Hu R, Chen Z, Dai C, Guo X, Feng W, Liu Z, Lin H, Chen Y, Wu R (2021) Engineering two-dimensional silicene composite nanosheets for dual-sensitized and photonic hyperthermia-augmented cancer radiotherapy. Biomaterials 269:120455.

Lee RHC, Lee MHH, Wu CYC, Couto ESA, Possoit HE, Hsieh TH, Minagar A, Lin HW (2018) Cerebral ischemia and neuroregeneration. Neural Regen Res 13:373-385.

Li C, Wang P, Tian Y, Xu X, Hou H, Wang M, Qi G, Jin Y (2017) Long-range plasmon field and plasmoelectric effect on catalysis revealed by shell-thickness-tunable pinhole-free Au@SiO2 core–shell nanoparticles: a case study of p-nitrophenol reduction. ACS Catal 7:5391-5398.

Liu Y, Kang N, Lv J, Zhou Z, Zhao Q, Ma L, Chen Z, Ren L, Nie L (2016) Deep photoacoustic/luminescence/magnetic resonance multimodal imaging in living subjects using high-efficiency upconversion nanocomposites. Adv Mater 28:6411-6419.

Longa EZ, Weinstein PR, Carlson S, Cummins R (1989) Reversible middle cerebral artery occlusion without craniectomy in rats. Stroke 20:84-91.

Ludwig PE, Thankam FG, Patil AA, Chamczuk AJ, Agrawal DK (2018) Brain injury and neural stem cells. Neural Regen Res 13:7-18.

Lutsep HL, Albers GW, DeCrespigny A, Kamat GN, Marks MP, Moseley ME (1997) Clinical utility of diffusion-weighted magnetic resonance imaging in the assessment of ischemic stroke. Ann Neurol 41:574-580.

Lv J, Peng Y, Li S, Guo Z, Zhao Q, Zhang X, Nie L (2018) Hemispherical photoacoustic imaging of myocardial infarction: in vivo detection and monitoring. Eur Radiol 28:2176-2183.

Ma J, Hong G, Ha E, Hong H, Kim J, Joo Y, Yoon S, Lyoo IK, Kim J (2021) Hippocampal cerebral blood flow increased following low-pressure hyperbaric oxygenation in firefighters with mild traumatic brain injury and emotional distress. Neurol Sci 42:4131-4138.

Nie L, Huang P, Li W, Yan X, Jin A, Wang Z, Tang Y, Wang S, Zhang X, Niu G, Chen X (2014) Early-stage imaging of nanocarrier-enhanced chemotherapy response in living subjects by scalable photoacoustic microscopy. ACS Nano 8:12141-12150.

Pang YQ, Yang J, Jia CM, Zhang R, Pang Q (2022) Hypoxic preconditioning reduces NLRP3 inflammasome expression and protects against cerebral ischemia/reperfusion injury. Neural Regen Res 17:395-400.

Provost C, Soudant M, Legrand L, Ben Hassen W, Xie Y, Soize S, Bourcier R, Benzakoun J, Edjlali M, Boulouis G, Raoult H, Guillemin F, Naggara O, Bracard S, Oppenheim C (2019) Magnetic resonance imaging or computed tomography before treatment in acute ischemic stroke. Stroke 50:659-664.

Rosenkrans ZT, Massey CF, Bernau K, Ferreira CA, Jeffery JJ, Schulte JJ, Moore M, Valla F, Batterton JM, Drake CR, McMillan AB, Sandbo N, Pirasteh A, Hernandez R (2022) [(68)Ga]Ga-FAPI-46 PET for non-invasive detection of pulmonary fibrosis disease activity. Eur J Nucl Med Mol Imaging doi: 10.1007/s00259-022-05814-9.

Ryu S, Yang YM, Yoo IS, Kim SW, Ha YR, Chung SP (2002) Comparison of diffusion-weighted and T2-weighted magnetic resonance imaging for ischemic stroke. J Korean Soc Emerg Med 13:111-115.

Saver JL, Starkman S, Eckstein M, Stratton SJ, Pratt FD, Hamilton S, Conwit R, Liebeskind DS, Sung G, Kramer I, Moreau G, Goldweber R, Sanossian N; FAST-MAG Investigators and Coordinators (2015) Prehospital use of magnesium sulfate as neuroprotection in acute stroke. N Engl J Med 372:528-536.

Schneider CA, Rasband WS, Eliceiri KW (2012) NIH Image to ImageJ: 25 years of image analysis. Nat Methods 9:671-675.

Silvestri L, van Saene HK, Rommes JH, Petros AJ, de la Cal MA, Bion JF (2017) Surviving Sepsis Campaign Guidelines 2016: omission of selective decontamination of the digestive tract deprives patients of a level 2B therapy. Minerva Anestesiol 83:1214-1215.

Taruttis A, Herzog E, Razansky D, Ntziachristos V (2010) Real-time imaging of cardiovascular dynamics and circulating gold nanorods with multispectral optoacoustic tomography. Opt Express 18:19592-19602.

Wang LV, Yao J (2016) A practical guide to photoacoustic tomography in the life sciences. Nat Methods 13:627-638.

Watson BD, Dietrich WD, Busto R, Wachtel MS, Ginsberg MD (1985) Induction of reproducible brain infarction by photochemically initiated thrombosis. Ann Neurol 17:497-504.

Wu H, Wang P, He H, Jin Y (2012) Controlled synthesis of porous Ag/Au bimetallic hollow nanoshells with tunable plasmonic and catalytic properties. Nano Res 5:135-144.

Wu MY, Yiang GT, Liao WT, Tsai AP, Cheng YL, Cheng PW, Li CY, Li CJ (2018) Current mechanistic concepts in ischemia and reperfusion injury. Cell Physiol Biochem 46:1650-1667.

Zemp RJ, Song L, Bitton R, Shung KK, Wang LV (2008) Realtime photoacoustic microscopy of murine cardiovascular dynamics. Opt Express 16:18551-18556.

Zhao W, Luo C, Wang J, Gong J, Li B, Gong Y, Wang J, Wang H (2014) 3-N-butylphthalide improves neuronal morphology after chronic cerebral ischemia. Neural Regen Res 9:719-726.

C-Editor: Zhao M; S-Editors: Yu J, Li CH; L-Editors: Yu J, Song LP; T-Editor: Jia Y